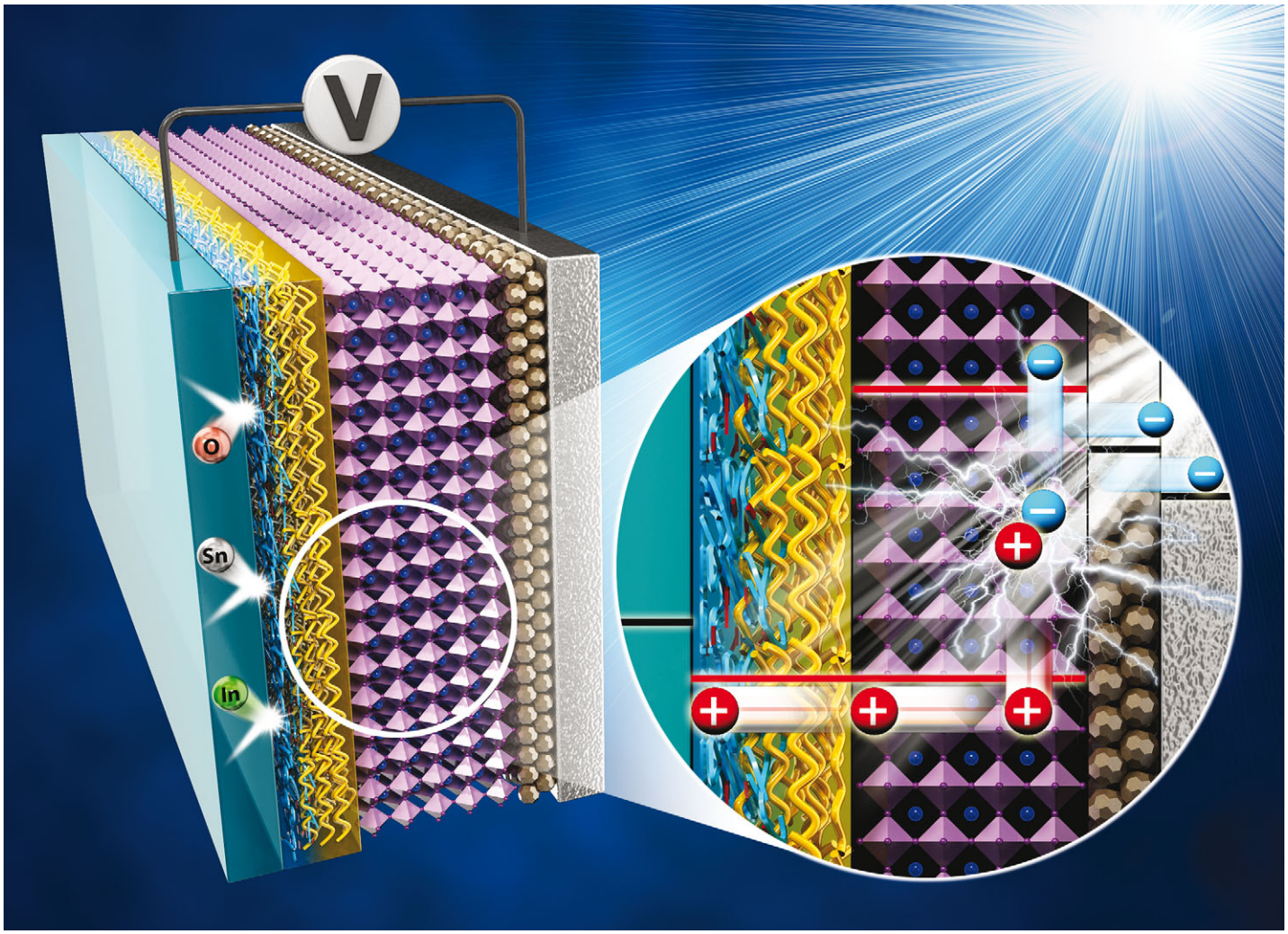

Showcasing research from Prof. Tae-Woo Lee's group at Pohang University of Science and Technology (POSTECH), Korea, and Prof. Yabing Qi's group at OIST, Japan.

Universal energy level tailoring of self-organized hole extraction layers in organic solar cells and organic–inorganic hybrid perovskite solar cells

Tailoring the interface energetics is crucially important to maximize device performance of organic solar cells and organic–inorganic hybrid perovskite solar cells. We systematically tailored the interface energy level of the self-organized hole extraction layer (SOHEL) to remove the energy offset at the interface and understand clearly the universal energy level alignment with the diverse photoactive materials. Furthermore, the operational stability is significantly prolonged due to the diffusion-blocking ability of the self-organized PFI at the surface of SOHELs for impurities from indium tin oxide.

Support acknowledged from CASE as Global Frontier Project 2014M3A6A5060947 and ADD UD140044GD.

As featured in:

See Tae-Woo Lee *et al.*, *Energy Environ. Sci.*, 2016, **9**, 932.

ROYAL SOCIETY OF CHEMISTRY

www.rsc.org/ees

Registered charity number: 207890

Energy & Environmental Science

PAPER

View Article Online
View Journal | View Issue

Cite this: *Energy Environ. Sci.*, 2016, **9**, 932

Universal energy level tailoring of self-organized hole extraction layers in organic solar cells and organic–inorganic hybrid perovskite solar cells†

Kyung-Geun Lim,[a] Soyeong Ahn,[a] Young-Hoon Kim,[a] Yabing Qi[b] and Tae-Woo Lee*[a]

Received 24th November 2015,
Accepted 13th January 2016

DOI: 10.1039/c5ee03560k

www.rsc.org/ees

Tailoring the interface energetics between a polymeric hole extraction layer (HEL) and a photoactive layer (PAL) in organic photovoltaics (OPVs) and organic–inorganic hybrid perovskite solar cells (PrSCs) is very important to maximize open circuit voltage (V_{oc}), power conversion efficiency (PCE), and device lifetime. In principle, when Fermi-level pinning and a vacuum level shift take place between the HEL and PAL, they give rise to an energy level offset between the HEL and the valence band maximum (VBM) (or the highly occupied molecular orbital (HOMO) in the case of organic photoactive materials) of the PAL and then V_{oc} loss. However, here we show that the V_{oc} loss at the interface can be overcome by universal energy level tailoring of a self-organized HEL (SOHEL) between the HEL and PAL irrespective of photoactive materials. A SOHEL composed of a conducting polymer and a perfluorinated ionomer (PFI) is effectively used to study the interface energetics in OPVs and PrSCs. We systematically tailored the interface energy level of the SOHEL to remove the energy offset at the interface and understand clearly the universal energy level alignment with the diverse photoactive materials of OPVs and PrSCs. The Fermi-level of the HEL is pinned to the midgap state of photoactive materials, which is about 0.6–0.7 eV above the VBM or HOMO. However, the interface energy state of the PFI-enriched surface layer of the SOHEL can be formed deeper below the Fermi-level by self-organized molecules so that it can match the top of the valence band of the photoactive materials. As a result, the energy offset at the interface between photoactive materials and the SOHEL can be significantly decreased to achieve high V_{oc} and PCE. Furthermore, our SOHEL significantly prolonged the stability of OPVs (half lifetime: 2.84 year) compared with pristine PEDOT:PSS (half lifetime: 0.2 year) under continuous irradiation of air mass-1.5 global simulated sunlight at 100 mW cm^{-2} due to the diffusion-blocking ability of the self-organized PFI at the surface of SOHELs for impurities from indium tin oxide.

Broader context

In this paper, we develop universal energy level tailoring at the hole extraction interface for organic and organic–inorganic hybrid perovskite photoactive layers (PALs) using self-organized polymeric hole extraction layers (SOHELs). We clearly show that although the Fermi-level of the conducting-polymer-based HEL is pinned to the mid-gap state of a PAL, the V_{oc} can be further increased and thus we can maximize the V_{oc} and power conversion efficiency (PCE) irrespective of Fermi-level pinning. Therefore, we can solve an important inherent and universal problem of potential loss at the hole extraction interface in organic photovoltaic cells (OPVs) and organic–inorganic hybrid perovskite solar cells (PrSCs). Furthermore, we demonstrate that the SOHEL can boost up the device lifetime significantly by 19 times. When we assume negligible degradation in the dark and 5.5 h of 1 sun intensity per day, the estimated operating half-lifetime of OPVs with SOHEL is 2.84 years. Our molecularly controlled strategies at the hole extraction interface provide a clear universal method to increase V_{oc}, PCE, and device lifetime.

[a] *Department of Materials Science and Engineering, Pohang University of Science and Technology (POSTECH), San 31 Hyoja-dong, Nam-gu, Pohang, Gyungbuk 790-784, Republic of Korea. E-mail: twlee@postech.ac.kr, taewlees@gmail.com*

[b] *Energy Materials and Surface Sciences Unit (EMSS), Okinawa Institute of Science and Technology Graduate University (OIST), 1919-1 Tancha, Onna-son, Kunigami-gun, Okinawa, 904-0495, Japan*

† Electronic supplementary information (ESI) available. See DOI: 10.1039/c5ee03560k

Introduction

Bulk heterojunction (BHJ) organic photovoltaic cells (OPVs)[1–11] and solution-processed planar heterojunction (SP-PHJ) organic–inorganic hybrid perovskite solar cells (PrSCs)[12–21] have been intensively studied due to their potential application in low-cost realization of flexible, printable, and portable solar cells.

There has been a remarkable progress of power conversion efficiency (PCE) in OPVs[11] and PrSCs.[21]

In spite of the difference in electronic properties between organic–inorganic perovskite and the organic photoactive layer, interfacial engineering at electrodes is one of the most crucial research topics in OPV and PrSC fields because it improves the device performance critically and enables the development of the reliable and flexible thin film solar cells.[5–9,20] Over the past decade, a number of research groups have revealed that the electrode interlayer significantly influences the important issues in the device such as built-in potential (V_{bi}),[5,9] device lifetime (LT),[5] charge carrier extraction,[7] and processability.[9,10] However there are few studies on the universal HEL material, which fully covers all important issues in solution processed OPVs and PrSCs. In addition, much less attention has been focused on systematic studies of precise energy alignment of the universal HEL in devices.

Transition-metal oxides (TMO) showed a universal energy-alignment trend with several organic semiconductors due to a broad range of work function (WF) from ~2 eV to ~7 eV.[22,23] Lu *et al.* observed that the energy alignment trend in various TMO (n-type wide-bandgap semiconductors, such as MoO_3, TiO_2, V_2O_5, WO_3 and Ta_2O_5; defective semiconducting oxides, such as MoO_{3-x}, TiO_{2-x}, V_2O_{5-x} and CrO_{3-x}; p-type semiconductors, such as Cu_2O, Ag_2O, Cr_2O_3 and Co_3O_4; p-type Mott–Hubbard insulators, such as CuO, NiO and CoO; and metallic oxides, such as MoO_2, WO_2 and TiO) with organic semiconductors stemming from electron chemical potential equilibration.[22] TMO can be widely used as the efficient charge extraction interlayer in OPVs and PrSCs, but they are almost a necessity to deposit different TMO materials by the vacuum deposition system for the energy alignment with each diverse semiconductor.

A self-organized HEL (SOHEL) can easily tune its energy levels with respect to the valance band maximum (VBM) or highly occupied molecular orbital (HOMO) of diverse photoactive materials.[20,24] This universal energy level alignment of the SOHEL can be controlled by relative concentrations of self-organized surface enriched molecules (*e.g.*, perfluorinated ionomer (PFI)) to a conducting polymer (*e.g.*, PEDOT:PSS) in the solution. Because PFI, *i.e.*, tetrafluoroethylene-perfluoro-3,6-dioxa-4-methyl-7-octene-sulfonic acid copolymer, is an additive polymer with the high ionization energy (IE) value and low surface energy that prefers to self-organize at the film surface, the surface WF of the SOHEL is increased as a function of the PFI/PEDOT:PSS molecular ratio.[20,24,25] Therefore the universal energy level tailoring of the SOHEL can reduce greatly the energy offset and charge recombination in the device with diverse photoactive layers.

Here, we systematically tailored the energy level of the SOHEL for the diverse photoactive materials of OPVs and PrSCs to improve the device performance and understand how the photovoltage is determined by the energy level alignment at the interface. We tried to elucidate the role of the universal energy level tailoring of the SOHEL for P3HT (poly(3-hexylthiophene-2,5-diyl)), PCDTBT (poly[*N*-9″-heptadecanyl-2,7-carbazole-*alt*-5,5-(4′,7′-di-2-thienyl-2′,1′,3′-benzothiadiazole)]), $MAPbI_3$ (methylammonium lead triiodide), and $MAPbBr_3$ (methylammonium lead tribromide) as the organic and organic–inorganic perovskite photoactive materials with various IE. We investigated the interface energy levels of the SOHEL and the energy offset at the SOHEL/photoactive layer (PAL) interface as a function of the PFI/PEDOT : PSS ratio in the SOHEL. The resulting open circuit voltage (V_{oc}) and the PCE of OPVs and PrSCs were also investigated depending on the energy level alignment at the interface. We additionally investigated the enhanced stability of OPVs with SOHELs compared with conventional PEDOT:PSS due to the diffusion-blocking ability of the self-organized PFI-enriched surface layer at the surface of SOHELs for impurities from indium tin oxide.[24] These approaches of interface engineering on solution processed SOHELs will be very useful to study for the impact of the universal energy level tailoring at the HEL/PAL interface on V_{oc} and give an insight on how one can minimize the potential loss and maximize the performance (PCE and LT) in OPVs and PrSCs.

Results and discussion

We employed the SOHELs to solution processed thin film solar cells with organic photoactive materials (P3HT and PCDTBT) or organic–inorganic hybrid perovskite photoactive materials ($MAPbI_3$ and $MAPbBr_3$), whose chemical structures are shown in Fig. S1 (ESI†). Because the WFs of SOHELs were controllable from 4.86 eV (pristine PEDOT:PSS) to 5.48 eV (SOHEL6) by varying the molecular ratio of PFI (Table 1), we expected the device with various photoactive materials to show the improved performance with SOHEL.

We fabricated the photovoltaic cells with SOHEL and measured the current density *versus* voltage (*J*–*V*) characteristics obtained under irradiation of air mass (AM)-1.5 global simulated sunlight at an intensity of 100 mW cm^{-2} (Fig. 1). When we used the SOHELs to the P3HT:$PC_{60}BM$ devices, we could not observe any noticeable increase of device performance in Fig. 1(a). However, the device performance of PCDTBT:$PC_{70}BM$ and $MAPbI_3$/$PC_{60}BM$ were significantly increased with SOHELs in Fig. 1(b) and (c). The PCDTBT:$PC_{70}BM$ device with SOHEL3 (WF = 5.32 eV) shows a higher V_{oc} (0.897 V) and J_{sc} (11.7 mA cm^{-2}) than the device based on pristine PEDOT:PSS (WF = 4.89 eV) (V_{oc} = 0.738 V; J_{sc} = 10.2 mA cm^{-2}). The $MAPbI_3$/$PC_{60}BM$ device with SOHEL5 (WF = 5.46 eV) shows a higher V_{oc} (1.03 V) and J_{sc} (15.7 mA cm^{-2}) than the device based on pristine PEDOT:PSS

Table 1 The polymer compositions and their work function levels of different SOHEL layers

Sample code	PEDOT : PSS : PFI	PFI/PEDOT : PSS	Work function [eV]
PEDOT:PSS	1 : 2.5 : 0	0	4.86
SOHEL1	1 : 2.5 : 0.1	0.027	5.11
SOHEL2	1 : 2.5 : 0.19	0.053	5.21
SOHEL3	1 : 2.5 : 0.37	0.105	5.32
SOHEL4	1 : 2.5 : 0.73	0.209	5.39
SOHEL5	1 : 2.5 : 1.5	0.417	5.46
SOHEL6	1 : 2.5 : 2.9	0.833	5.48

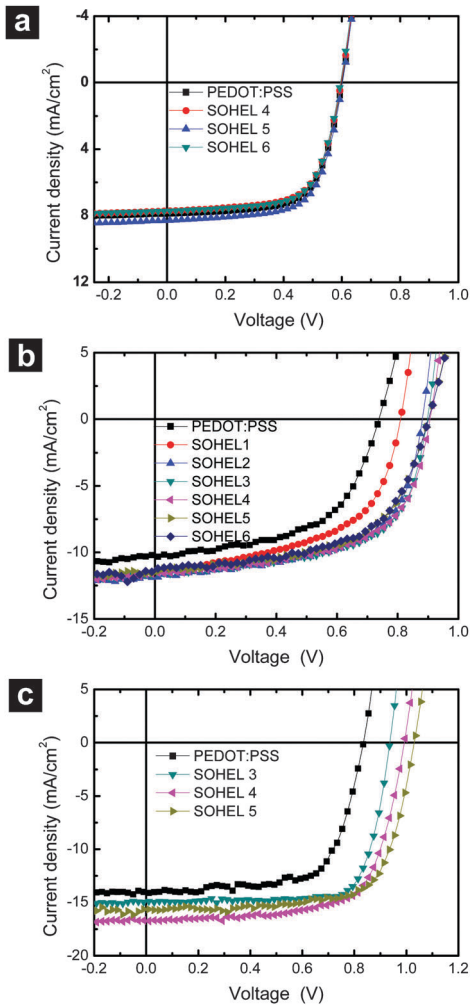

Fig. 1 The *J*–*V* characteristics of (a) P3HT:$PC_{60}BM$, (b) PCDTBT:$PC_{70}BM$ organic photovoltaics and (c) $MAPbI_3$/$PC_{60}BM$ perovskite solar cells with the PEDOT:PSS (■), SOHEL1 (●), SOHEL2 (▲), SOHEL3 (▼), SOHEL4 (◀), SOHEL5 (▶), and SOHEL6 (◆) as the hole extraction layers under irradiation of AM-1.5 100 mW cm^{-2}.

(WF = 4.89 eV) (V_{oc} = 0.835 V; J_{sc} = 14.1 mA cm^{-2}) (Tables S1 and S2, ESI†). The device results of SOHEL/$MAPbI_3$ are compiled from ref. 20.

When the WF of the HEL is well aligned with the VBM or HOMO of photoactive materials, the potential energy loss at the interface will be minimized and thus V_{bi} increases.[20] Compared with conventional PEDOT:PSS, the SOHEL was used as the high WF hole extraction material, therefore the energy offset at the hole extraction interface was decreased in the device with photoactive materials with a deep lying HOMO level (*e.g.* PCDTBT and $MAPbI_3$). Schematic diagram of the energy levels of photoactive materials is drawn in Fig. S2 (ESI†). As a result, the energy level offset at the SOHEL/PCDTBT:$PC_{70}BM$ interface decreased and the V_{bi} and V_{oc} of the device increased accordingly[26,27] depending on the WF of the SOHEL (Fig. 1(b)). In the same manner, the V_{oc} of the $MAPbI_3$ (−5.4 eV) and $MAPbBr_3$ (−5.9 eV) perovskite solar cells with a SOHEL device increased compared to those with PEDOT:PSS due to the good energy alignment of the SOHEL with the $MAPbI_3$ and

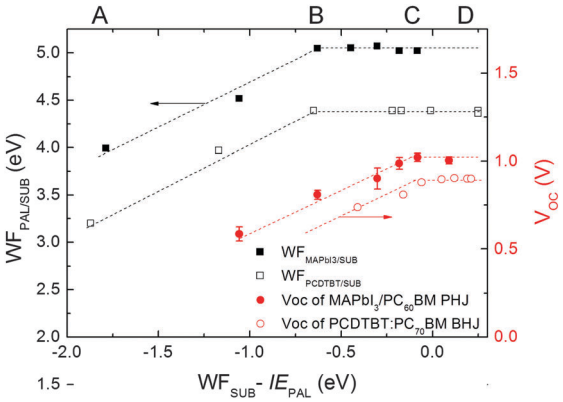

Fig. 2 Open circuit voltage of the $MAPbI_3$/$PC_{60}BM$ device (filled) and the PCDTBT:$PC_{70}BM$ device (open) and the work function of them *versus* the difference of the conducting substrate work function (WF_{SUB}) and ionization energy of the active layer (IE_{PAL}). Glass/Al (3.4 eV), ITO/ODT-SAM (4.1 eV), PEDOT:PSS and a SOHEL (4.6–5.5 eV) were used as the conducting substrate. (WF results are shown in Fig. S4 and S5, ESI.†)

$MAPbBr_3$ layer (Fig. 1(c) and Fig. S3, ESI†). On the other hand, PEDOT:PSS is already well aligned with the HOMO level of the P3HT (−4.8 eV), thus no significant differences of V_{oc} were found in the P3HT:$PC_{60}BM$ device with high WF SOHELs in Fig. 1(a).

We systematically investigated energy level alignment and corresponding V_{oc} of PCDTBT:$PC_{70}BM$ and $MAPbI_3$/$PC_{60}BM$ devices depending on various WFs of the HEL. The WF of the PAL on the substrate ($WF_{PAL/SUB}$) and corresponding V_{oc} is plotted against the substrate WF (WF_{SUB}) (Fig. 2). Glass/Al (3.4 eV) and ITO/ODT-SAM (4.1 eV), glass/ITO (4.3 eV), glass/ITO/PEDOT:PSS (4.6 eV), and glass/ITO/SOHEL (5.1–5.5 eV) were used as the conducting substrate with various WF_{SUB}. These WF data are extracted from ultraviolet photoemission spectroscopy (UPS) results (Fig. S4 and S5, ESI†). In the A–B regime of Fig. 2, the WF of PCDTBT ($WF_{PCDTBT/SUB}$) and $MAPbI_3$ ($WF_{MAPbI_3/SUB}$) linearly increased depending on WF_{SUB}. The slope parameter $S = dWF_{PAL/SUB}/dWF_{SUB}$, which is used to characterize the energetics of the interfaces, equals 1. This A–B regime of linear dependence corresponds to the vacuum level alignment regime (Schottky–Mott limit),[28] which corresponds to the situation where the E_F of the substrate lies within the HOMO–LUMO (or VBM-conduction band maximum) gap of the PAL and the HOMO (or VBM) level of the PAL is well below the Fermi-level of the substrate, and hence no net charge exchange occurs between the substrate and PAL. Therefore, the Schottky barrier or energy offset at the interface is inversely proportional to WF_{SUB}. However when the WF_{SUB} is increased further, $WF_{PAL/SUB}$ reaches a value that is ~0.7 eV shallower than the HOMO or VBM level of PALs and remains constant with further increases in WF_{SUB}. Thus $WF_{PCDTBT/SUB}$ and $WF_{Perovskite/SUB}$ become independent of WF_{SUB} in the B–D regime and slope S is changed to 0 (S = 0) due to Fermi-level pinning.[22,29–31] We should note that the Fermi-level is pinned at the energy state that lies within the HOMO–LUMO gap and ~0.7 eV shallower than the HOMO or VBM level of PALs. These midgap states (called the trap state, charge transfer state,[32,33]

bipolaron state,[32,34–36] charge neutrality level (CNL)[32,36,37] or integer charge transfer (ICT) state[23,32,36,38–40]) in photoactive polymers (*e.g.* P3HT, PCDTBT) are well defined as the energy required to take away one electron from the molecule producing a fully relaxed state (*i.e.* both electronic and geometrical relaxation are included) and created upon oxidation of the molecules at the interface. The magnitude of energy difference between the midgap state and HOMO is reported to be 0.4–0.7 eV in P3HT, TFB, P10AF and PFO because the π-band edge of a conjugated polymer remains at a constant distance in energy from the Fermi-level of the substrate.[36] The ICT model further predicts that Fermi-level pinning to the E_{ICT} of the semiconductor occurs when WF_{SUB} has exceeded the E_{ICT} level.[23,32,36,38–40]

The midgap states in perovskite have also been reported recently and intensively studied.[41–50] This midgap state of perovskite stems from the state of anti-site defects with I occupying a CH_3NH_3 site[44–46] or the exponential tail states (also called the Urbach tail).[47] Snaith *et al.* reported a significant population of the subgap states of flat PHJ $MAPbI_3$ perovskite compared with meso-superstructured $MAPbI_3$ perovskite.[41] In the same manner, we analyzed the UPS spectrum on a logarithm scale and detected a very low density of gap state near the VBM of $MAPbI_3$. In Fig. 3, the dashed curve is the Gaussian function of density of state formed at the lowest binding energy of $MAPbI_3$ perovskite and the arrow represents the boundary of the exponential distribution of the gap state. These results demonstrate that the exponential tail state appears as the midgap state, which is located above the boundary edge of the Gaussian density of state of the valence band and within the band gap of $MAPbI_3$ perovskite.

The device parameter determined from energy alignment at the interface, V_{oc}, of PCDTBT:$PC_{70}BM$ and the $MAPbI_3$/$PC_{60}BM$ perovskite device tends to increase linearly as a function of WF_{SUB} in the Schottky–Mott regime (A–B regime in Fig. 2), because the energy offset at the interface is decreased and thus V_{bi} increases in the device. Once V_{oc} becomes a maximum value, it remains a constant with WF_{SUB} due to Fermi-level pinning in the C–D regime. However, V_{oc} of the device with SOHEL keeps increasing as a function of WF_{SUB} increasing in the B–C regime, even though the Fermi-level of the HEL is pinned to the midgap state of photoactive materials. Although the Schottky barrier at the interface remains constant when the E_F pinning occurs at the interface (slope parameter of WF_{PAL} $S = 0$), V_{oc} of the device increases from 0.738 V to 0.904 V (PCDTBT) and 0.835 V to 1.030 V ($MAPbI_3$ perovskite). So, we investigated the electronic structure of the SOHEL to provide the energy level alignment at the interface and the V_{oc} increasing mechanism for the device with SOHELs.

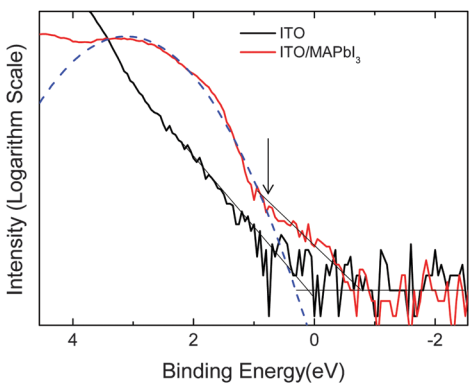

Fig. 3 Ultraviolet photoelectron spectroscopy spectra of ITO and $MAPbI_3$ perovskite thin films on ITO. The arrows correspond to an exponential tail state of $MAPbI_3$.

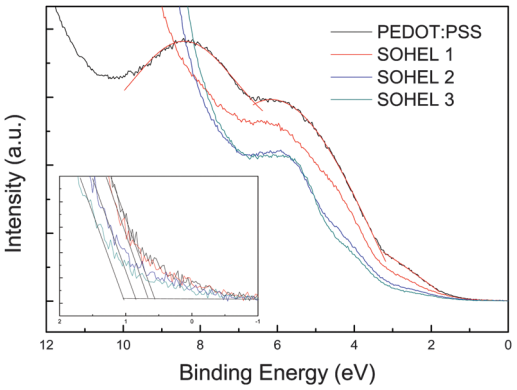

Fig. 4 Ultraviolet photoelectron spectroscopy spectra of PEDOT:PSS and the SOHEL. Inset shows the interfacial energy states of the SOHEL formed at a deeper level than at the Fermi-level.

We compared the UPS spectra of PEDOT:PSS and the SOHEL to investigate the density of states around the Fermi-level and different electronic structures induced by a surface-enriched polymeric dopant layer (Fig. 4). Much work has been devoted to understand great electrical properties of PEDOT:PSS in organic electronics over the past few decades. PSS molecules tend to be located at the surface due to the low surface energy and this surface-enriched PSS layer on the PEDOT:PSS film can control the WF of the surface.[10,51,52] When a surface-enriched PSS layer was removed by light argon sputtering, the energy state was occupied with electrons up to E_F as expected for a heavily p-doped PEDOT layer. However, the as-loaded PEDOT:PSS films without light argon sputtering show that the unoccupied energy state extended to 0.25 eV below the E_F, called the interfacial energy state (IES).[51] It is because the surface-enriched dopant layer (PSS) suppresses and reduces the density of states of the bulk PEDOT:PSS layer so that it induces the interfacial energy state below the Fermi-level.[51] We found the density of state of the SOHEL near the E_F decreased more compared with PEDOT:PSS (Fig. 4), thus the IES of the SOHEL is formed at a deeper level than that of PEDOT:PSS (inset). In XPS depth profiling of PEDOT:PSS and the SOHEL, the fluorocarbon chains (CF_2) in PFI molecules are mostly rich at the SOHEL surface compared with PSS molecules.[20] Because the IE value of PFI molecules is larger than that of PSS molecules,[24,53] the surface-enriched PFI molecules in the SOHEL induce more unfilled state and much deeper level of the IES depending on the PFI/PEDOT : PSS ratio of the SOHEL. As a result, when the SOHEL contacts photoactive materials (PCDTBT or $MAPbI_3$), the IES of the SOHEL can reach closer to the HOMO or VBM of photoactive materials compared with that of PEDOT:PSS to

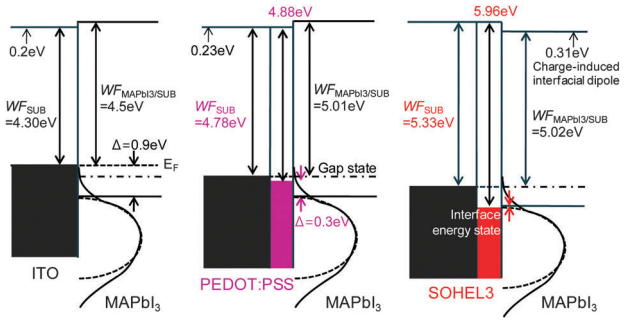

Fig. 5 Schematic diagrams of the energy level at the ITO/$MAPbI_3$, PEDOT:PSS/$MAPbI_3$, and SOHEL/$MAPbI_3$ interface.

reduce the energy offset and increase the corresponding V_{oc} in the device, even though the E_F of the SOHEL is pinned at the midgap state of photoactive materials (B–C regime of Fig. 2).

The results for the interfaces between $MAPbI_3$ perovskite and HELs are summarized in Fig. 5 by the schematic diagrams of the energy level alignment at the interface between $MAPbI_3$ perovskite with various substrates of ITO, PEDOT:PSS or the SOHEL. At the ITO/$MAPbI_3$ interface, the energy level offset between WF_{SUB} and VBM of $MAPbI_3$ is 0.9 eV due to relatively low WF_{SUB} of ITO. At the PEDOT:PSS/$MAPbI_3$ interface, WF_{SUB} is increased to 4.78 eV and the Fermi-level of the PEDOT:PSS approaches the VBM of the $MAPbI_3$, thus the resulting WF of $MAPbI_3$ is increased to 5.01 eV. However the WF of $MAPbI_3$ is not changed in further increased WF_{SUB} of the SOHEL (5.33 eV), because the Fermi-level was pinned at the midgap state of the $MAPbI_3$. When the energy level of the midgap state is shallower than WF_{SUB}, electrons of the midgap state are transferred to the substrate across the interface until equilibrium is reached. This charge transfer across the interface results in the creation of an charge-transfer-induced interfacial dipole that upshifts the vacuum level when charges are transferred to the substrate.[54,55] A charge-transfer-induced interfacial dipole is formed at the SOHEL/$MAPbI_3$ interface and it increases depending on the PFI/PEDOT : PSS ratio in the SOHEL. It is because more electrons should be transferred across the interface to the deeper IES of the SOHEL compared with PEDOT:PSS until equilibrium is reached. We also found that the electrons of $MAPbI_3$ perovskite transferred to the adjacent HEL depending on the energy alignment at the interface. In UPS spectra, the density of state near the VBM of $MAPbI_3$ was reduced with increasing WF and deepening IES of the HEL (Fig. S6, ESI†), because more electrons should be transferred across the interface to the HEL with deeper IES to reach equilibrium. In the same manner, the energy diagrams of P3HT, PCDTBT, and $MAPbBr_3$ are summarized in Fig. S7–S9 (ESI†), respectively.

We measured the electrical and optical properties of SOHELs and investigated the device characteristics based on SOHELs. The electrical and optical properties of SOHELs are comparable with those of PEDOT:PSS. The conductivities of 20 nm-thick PEDOT:PSS and SOHEL4 films are 4.9×10^{-1} S cm^{-1} and 4.7×10^{-1} S cm^{-1}, respectively. The transmittance spectra of PEDOT:PSS and SOHEL4 were almost identical as shown in Fig. S10 (ESI†). On the other hand, the rectification ratio (forward-biased current/reverse-biased current) at ±2.0 V in the dark *J–V* characteristic curve of the $MAPbI_3$ device increased from 8.2×10^2 (PEDOT:PSS) to 3.3×10^3 (SOHEL4) and 7.6×10^3 (SOHEL5) (Fig. S11, ESI†). It apparently shows that the conductivity and transmittance of SOHELs are very similar to those of PEDOT:PSS, while the energy level of the SOHEL is significantly modified to form the ohmic contact at the interface. We used the Clevios PH with lower PSS molecular ratio (*e.g.* PEDOT : PSS = 1 : 2.5) to achieve highly conductive PEDOT:PSS:PFI as a SOHEL despite lower WF (4.9 eV in Table 1) of Clevios PH compared with that of Clevios P VP AI4083 with a higher PSS molecular ratio (*e.g.* PEDOT : PSS = 1 : 6) which showed a conductivity of $\sim 6 \times 10^{-4}$ S cm^{-1} [24,52,56] and a WF of 5.2 eV.[24,52,56,57] Our SOHELs based on Clevios PH showed a higher WF (up to 5.48 eV in Table 1) and a higher conductivity (4.7×10^{-1} S cm^{-1} for SOHEL4) than those of Clevios P VP AI4083 because of the lower PSS concentration and higher PFI concentration in the composition. The built-in potential[20] and V_{oc} of the device based on the SOHEL increased compared with those of the PEDOT:PSS-based device due to a good energy level alignment of the SOHEL with the HOMO or VBM level of photoactive materials. Therefore, the photocurrent was easily extracted to the electrodes in the PCDTBT and $MAPbI_3$ solar cells based on the SOHEL and the resulting J_{sc} increased compared with that of the PEDOT:PSS-based device (Tables S1 and S2, ESI†).

The quality of $MAPbI_3$ films on PEDOT:PSS and the SOHEL was investigated using X-ray diffraction (XRD), field-emission scanning electron microscopy (SEM), and transient photoluminescence (Tr-PL) spectroscopy (Fig. S12–S14, ESI,† respectively). We investigated the [110] diffraction peaks of $MAPbI_3$ perovskite and the [001] diffraction peaks of PbI_2 in XRD patterns (Fig. S12, ESI†), however we could not find a noticeable change in the peak positions of [110] and [001] diffraction peaks and their full-width half-maximum (FWHM) of both samples depending on the substrates (Table S3, ESI†). The crystalline structure and crystallinity of $MAPbI_3$ perovskite and the unreacted PbI_2 were not changed depending on HELs. We also estimated the morphology of $MAPbI_3$ film repeatedly for a relatively rough surface of $MAPbI_3$ film due to its rapid crystal growth. In high magnification (×30k) SEM images (Fig. S13, ESI†), we could not estimate the noticeable changes in the surface morphologies such as grain size or the number of pin-hole of $MAPbI_3$ perovskite films depending on substrates. Since the crystal structure of $MAPbI_3$ is constructed by the intercalation of MAI molecules into PbI_2 crystalline during sequential deposition of MAI casting on PbI_2 film, the crystallization and morphology of $MAPbI_3$ are rarely affected by the surface properties the of HEL in case of a two-step process. The average PL lifetime (τ_{avr}) of PEDOT:PSS/$MAPbI_3$, SOHEL3/$MAPbI_3$ and SOHEL5/$MAPbI_3$ are 17.71, 18.746 and 19.634 ns, respectively (Fig. S14, ESI†). These similar lifetimes confirm that the $MAPbI_3$ layer fabricated on different under-layers showed similar morphology and grain size. However, gradually increasing the PL lifetime of $MAPbI_3$ from PEDOT:PSS to SOHEL5 originated from the blocking of the quenching of electron–hole pairs at the HEL/$MAPbI_3$ interface due to the surface-enriched PFI layer of the SOHEL.

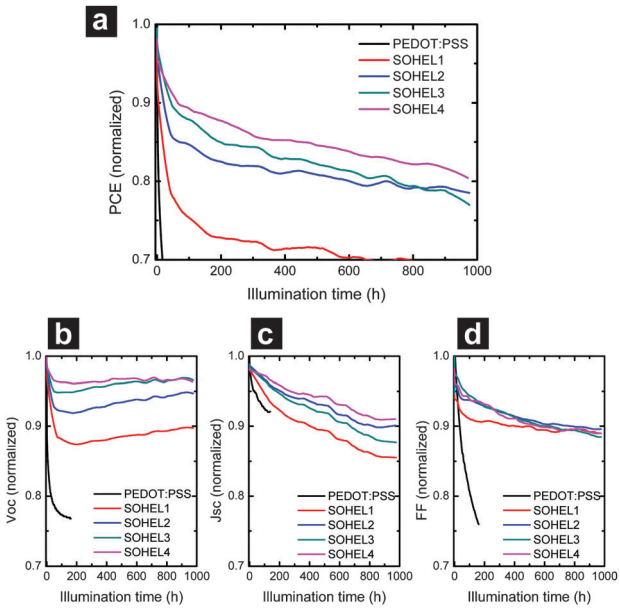

Fig. 6 Stability measurement of the SOHEL/PCDTBT:$PC_{70}BM$ device kept under continuous simulated solar irradiation at 100 mW cm^{-2} and 25.3 °C. (a) PCEs of devices with different PFI ratios were compared over time. Comparison of performance parameters of (b) V_{oc}, (c) J_{sc} and (d) FF of the continuously illuminated device.

We investigated the LT of OPVs by measuring the PCE of devices over time under continuous irradiation of 100 mW cm^{-2} simulated sunlight at 25.3 °C in Fig. 6. The LT of PCDTBT:$PC_{70}BM$ solar cells that employ SOHELs was significantly longer than that of the conventional PEDOT:PSS device, and significantly increased as a function of the PFI/PEDOT : PSS ratio in SOHELs. The half-LT of the device with pristine PEDOT:PSS was 300 h. It is increased to 4200 h (SOHEL1) and 5700 h (SOHEL4) in the extrapolation slope. When we assume negligible degradation of OPVs in the dark and 5.5 h of 1 sun intensity per a day,[58] the estimated operating half-LT of the PCDTBT:$PC_{70}BM$ device with PEDOT:PSS and SOHEL4 is 0.15 and 2.84 years, respectively. A major reason for the LT prolongation is the diffusion-blocking ability of the self-organized fluorocarbon layer at the surface of our SOHELs for the impurities (*e.g.* sulfates, alkali metals, In atoms, and Sn atoms) from ITO.[24] This diffusion-blocking ability is increased with the PFI molecular ratio in the SOHEL because the fluorocarbon chains in the PFI show good chemical stability and hydrophobicity and tend to be preferentially organized as a surface-enriched overlayer.[53] The V_{oc} of the device tended to deteriorate more significantly than did J_{sc} (Fig. 6b and c); this indicates that an impurity diffusion blocking layer of PFI is important to maintain V_{bi} during device operation under illumination.

Experimental

Device fabrication

A solution of PEDOT:PSS (Clevios™ PH) was mixed with 5 wt% tetrafluoroethylene-perfluoro-3,6-dioxa-4-methyl-7-octene-sulfonic acid copolymer (a perfluorinated ionomer) (Sigma Aldrich Co.) in various weight ratios (Table 1) and spin-coated as hole extraction layers (35 nm thick) on top of indium-tin-oxide (ITO)/glass. The weight ratio of PEDOT : PSS to PFI in the solution was varied as 128 : 1 (SOHEL1), 64 : 1 (SOHEL2), 32 : 1 (SOHEL3), 16 : 1 (SOHEL4), 8 : 1 (SOHEL5) and 4 : 1 (SOHEL6). The SOHEL was baked on a hotplate in air at 150 °C for 10 min. The substrates were moved to a N_2 glove box, then P3HT (Rieke Metals Inc., P200): $PC_{60}BM$ (nano-C Inc.): dichlorobenzene (Sigma-Aldrich Inc., Anhydrous) (20 mg: 20 mg: 1.5 mL) or PCDTBT (1material Inc.): $PC_{70}BM$ (nano-C Inc.): dichlorobenzene (Sigma-Aldrich Inc., Anhydrous) (7 mg: 28 mg: 1 mL) solution which had been heated for 6 h at 60 °C were spin-coated on the hole extraction layers to thicknesses of 210 nm and 75 nm, respectively. P3HT:$PC_{60}BM$ thin films were dried slowly and baked at 150 °C for 30 min on a vacuum hotplate to arrange the molecular ordering; PCDTBT:$PC_{70}BM$ thin films were baked at 70 °C for 10 min. Then cathodes were thermally evaporated on the photoactive layer surface in a vacuum of 2×10^{-7} Torr. First a 3 nm-thick Ba or Ca interfacial cathode was deposited at 0.1 Å s^{-1}. Then a 20 nm-thick Al cathode layer was deposited at 1 Å s^{-1} and an 80 nm-thick Al cathode layer was deposited at 5 Å s^{-1} sequentially. For perovskite solar cells, the substrates were moved to a N_2 glove box, then a PbI_2 layer was spin cast from 17.2 wt% PbI_2 solution in anhydrous *N*,*N*-dimethylformamide (DMF) (Aldrich) with a spin-coating speed of 8000 rpm for 30 s, followed by thermal annealing at 70 °C for 10 min. Then CH_3NH_3I was deposited from 20 mg mL^{-1} CH_3NH_3I solution in anhydrous IPA with a spin-coating speed of 3000 rpm for 30 s; the film immediately darkened after the CH_3NH_3I solution was added. The coated films were then placed on a hot plate set at 100 °C for 5 min. The $PC_{60}BM$ layer was spin-coated from 0.7 wt% $PC_{60}BM$ (nano-C Inc.) solution in chloroform, then cathodes were thermally evaporated on the photoactive layer surface in a vacuum (2×10^{-7} Torr). A 20 nm-thick Al cathode layer was deposited at 1 Å s^{-1} and an 80 nm-thick Al cathode layer was deposited at 3 Å s^{-1} sequentially without a Ca interlayer.[20] The photoactive area (0.06 cm^2) was determined using metallic shadow masks. In the N_2 glove box, a UV-curable epoxy resin was used to encapsulate the devices with a glass lid.

Characterization

The current density–voltage characteristics (*J*–*V* curves) were obtained using a Keithley 2400 source measurement unit under irradiation at AM-1.5 100 mW cm^{-2} generated using a Newport 69907 solar simulator.

The stability of the devices was measured using a McScience Polaronix K3600 Solar Cell Reliability Test System. Device characteristics were recorded at intervals of <1 h under irradiance of AM-1.5 100 mW cm^{-2} light and 25.3 °C until the PCE had decreased by 50% until half-lifetime.

The WF and VBM or HOMO of the surface was measured using an ultraviolet photoelectron spectroscopy (UPS). All measurements were conducted at room temperature.

To measure the PL decays of perovskite films, we used a picosecond pulsed laser head (LDH-P-C-405B, PicoQuant) as a 405 nm excitation source and a PDL800-D (PicoQuant) laser driver.

The PL lifetime was resolved and measured by using a monochromator (SP-2155, Acton) and a MCP-PMT (R3809U-50, Hamamatsu). We also used a PicoHarp 300 TCSPC module (PicoQuant GmbH) to calculate the PL lifetime from PL decay curves.

Conclusions

We systematically demonstrate that the energy offset at the HEL/PAL interface in OPVs and PrSCs can be eliminated by universal energy level tailoring of the SOHEL. We can control WF and the IES level of the SOHEL *via* the surface-enriched PFI molecule. Although the Fermi-level of HELs tends to be pinned to the midgap state of PALs, the IES of the SOHEL can be aligned with the HOMO or VBM level of PALs and thus the V_{oc} can be increased further even after Fermi-level pinning. Therefore, we can use universal energy level tailoring of the SOHEL for various organic and perovskite PAL materials with diversed HOMO or VBM levels, minimize the potential loss at the hole extraction interface, and then maximize V_{oc} in the OPVs and PrSCs with the SOHEL. Furthermore, SOHELs significantly prolonged the half-LT of the OPVs by 19 times under continuous irradiation of AM-1.5 100 mW cm^{-2} simulated sunlight at 25.3 °C because of the self-organized fluorocarbon molecules at the SOHEL surface which has good chemical stability and hydrophobicity. All the results clearly support that the SOHEL is a multi-functional and universal HEL material for highly efficient and reliable OPVs and PrSCs.

Acknowledgements

This work was supported by the Center for Advanced Soft-Electronics funded by the Ministry of Science, ICT and Future Planning as Global Frontier Project (2014M3A6A5060947) and the Agency for Defense Development (UD140044GD), Republic of Korea. Y. B. Qi would like to thank the funding from the Energy Materials and Surface Sciences Unit of the Okinawa Institute of Science and Technology Graduate University.

References

1 L. Chen, Z. Hong, G. Li and Y. Yang, *Adv. Mater.*, 2009, **21**, 1434.
2 G. Dennler, M. C. Scharber and C. J. Brabec, *Adv. Mater.*, 2009, **21**, 1323.
3 W. Ma, C. Yang, X. Gong, K. Lee and A.-J. Heeger, *Adv. Funct. Mater.*, 2005, **15**, 1617.
4 J. Peet, A. J. Heeger and G. C. Bazan, *Acc. Chem. Res.*, 2009, **42**, 1700.
5 K.-G. Lim, M.-R. Choi, J. H. Kim, D. H. Kim, G. H. Jung, Y. Park, J.-L. Lee and T.-W. Lee, *ChemSusChem*, 2014, **7**, 1125.
6 S. Kwon, K.-G. Lim, M. Shim, H. C. Moon, J. Park, G. Jeon, J. Shin, K. Cho, T.-W. Lee and J. K. Kim, *J. Mater. Chem. A*, 2013, **1**, 11802.
7 G. H. Jung, K.-G. Lim, T.-W. Lee and J.-L. Lee, *Sol. Energy Mater. Sol. Cells*, 2011, **95**, 1146.
8 K.-G. Lim, J.-M. Park, H. Mangold, F. Laquai, T.-L. Choi and T.-W. Lee, *ChemSusChem*, 2015, **8**, 337.
9 K.-G. Lim, M.-R. Choi, H.-B. Kim, J. H. Park and T.-W. Lee, *J. Mater. Chem.*, 2012, **22**, 25148.
10 D.-H. Kim, K.-G. Lim, J. H. Park and T.-W. Lee, *ChemSusChem*, 2012, **5**, 2053.
11 C.-C. Chen, W.-H. Chang, K. Yoshimura, K. Ohya, J. You, J. Gao, Z. Hong and Y. Yang, *Adv. Mater.*, 2014, **26**, 5670.
12 A. Kojima, K. Teshima, Y. Shirai and T. Miyasaka, *J. Am. Chem. Soc.*, 2009, **131**, 6050.
13 H. S. Kim, J. W. Lee, N. Yantara, P. P. Boix, S. A. Kulkarni, S. Mhaisalkar, M. Grätzel and N. G. Park, *Nano Lett.*, 2013, **13**, 2412.
14 J. H. Heo, S. H. Im, J. H. Noh, T. N. Mandal, C. S. Lim, J. A. Chang, Y. H. Lee, H. Kim, A. Sarkar, M. K. Nazeeruddin, M. Grätzel and S. I. Seok, *Nat. Photonics*, 2013, **7**, 486.
15 J. Burschka, N. Pellet, S.-J. Moon, R. Humphry-Baker, P. Gao, M. K. Nazeeruddin and M. Grätzel, *Nature*, 2013, **499**, 316.
16 M. M. Lee, J. Teuscher, T. Miyasaka, T. N. Murakami and H. J. Snaith, *Science*, 2012, **338**, 643.
17 M. Liu, M. B. Johnston and H. J. Snaith, *Nature*, 2013, **501**, 395.
18 P.-W. Liang, C.-Y. Liao, C.-C. Chueh, F. Zuo, S. T. Williams, X.-K. Xin, J. Lin and A. K.-Y. Jen, *Adv. Mater.*, 2014, **26**, 3748.
19 G. E. Eperon, V. M. Burlakov, P. Docampo, A. Goriely and H. J. Snaith, *Adv. Funct. Mater.*, 2014, **24**, 151.
20 K.-G. Lim, H.-B. Kim, J. Jeong, H. Kim, J. Y. Kim and T.-W. Lee, *Adv. Mater.*, 2014, **26**, 6461.
21 W. S. Yang, J. H. Noh, N. J. Jeon, Y. C. Kim, S. Ryu, J. Seo and S. I. Seok, *Science*, 2015, **348**, 1234.
22 M. T. Greiner, M. G. Helander, W.-M. Tang, Z.-B. Wang, J. Qiu and Z.-H. Lu, *Nat. Mater.*, 2012, **11**, 76.
23 L. Ley, Y. Smets, C. I. Pakes and J. Ristein, *Adv. Funct. Mater.*, 2013, **23**, 794.
24 T.-W. Lee, Y. Chung, O. Kwon and J. J. Park, *Adv. Funct. Mater.*, 2007, **17**, 390.
25 H. Cho, S.-H. Jeong, M.-H. Park, Y.-H. Kim, C. Wolf, C.-L. Lee, J. H. Heo, A. Sadhanala, N. Myoung, S. Yoo, S. H. Im, R. H. Friend and T.-W. Lee, *Science*, 2015, **350**, 1222; Y.-H. Kim, H. Cho, J. H. Heo, T.-S. Kim, N. Myoung, C.-L. Lee, S. H. Im and T.-W. Lee, *Adv. Mater*, 2015, **27**, 1248; K.-G. Lim, S. Ahn, H. Kim, M.-R. Choi, D. H. Huh and T.-W. Lee, *Adv. Mater. Int.*, 2016, DOI: 10.1002/admi.201500678.
26 V. D. Mihailetchi, P. W. M. Blom, J. C. Hummelen and M. T. Rispens, *J. Appl. Phys.*, 2003, **94**, 6849.
27 T. M. Brown, R. H. Friend, I. S. Millard, D. J. Lacey, T. Butler, J. H. Burroughes and F. Cacialli, *J. Appl. Phys.*, 2003, **93**, 6195.
28 S. Davids, A. Saxena and D. L. Smith, *J. Appl. Phys.*, 1995, **78**, 4244.
29 C. Tengstedt, W. Osikowicz, W. R. Slaneck, I. D. Parker, C. Hsu and M. Fahlman, *Appl. Phys. Lett.*, 2006, **88**, 053502.
30 H. Aarnio, P. Sehati, S. Braun, M. Nyman, M. P. Jong, M. Fahlman and R. Osterbacka, *Adv. Energy Mater.*, 2011, **1**, 792.

31 N. Koch and A. Vollmer, *Appl. Phys. Lett.*, 2006, **89**, 162107.
32 J. Hwang, A. Wan and A. Kahn, *Mater. Sci. Eng.*, 2009, **64**, 1.
33 T. M. Burke, S. Sweetnam, K. Vandewal and M. D. McGehee, *Adv. Energy Mater.*, 2015, **5**, 1500123.
34 W. R. Salaneck, R. H. Friend and J. L. Bredas, *Phys. Rep.*, 1999, **319**, 231.
35 C. Tengstedt, W. Osikowicz, W. R. Slaneck, I. D. Parker, C. Hsu and M. Fahlman, *Appl. Phys. Lett.*, 2006, **88**, 053502.
36 S. Braun, W. R. Salaneck and M. Fahlman, *Adv. Mater.*, 2009, **21**, 1450.
37 H. Vazquez, F. Flores and A. Kahn, *Org. Electron.*, 2007, **8**, 241.
38 H. Aarnio, P. Sehati, S. Braun, M. Nyman, M. P. de Jong, M. Fahlman and R. Österbacka, *Adv. Energy Mater.*, 2011, **1**, 792.
39 Z. Xu, L.-M. Chen, M.-H. Chen, G. Li and Y. Yang, *Appl. Phys. Lett.*, 2009, **95**, 013301.
40 M. Bokdam, D. Cakir and G. Brocks, *Appl. Phys. Lett.*, 2011, **98**, 113303.
41 T. Leijtens, S. D. Stranks, G. E. Eperon, R. Lindblad, E. M. J. Johansson, I. J. McPherson, H. Rensmo, J. M. Ball, M. M. Lee and H. J. Snaith, *ACS Nano*, 2014, **8**, 7147.
42 Y. Shao, Z. Xiao, C. Bi, Y. Yuan and J. Huang, *Nat. Commun.*, 2014, **5**, 5784.
43 D. Shi, V. Adinolfi, R. Comin, M. Yuan, E. Alarousu, A. Buin, Y. Chen, S. Hoogland, A. Rothenberger, K. Katsiev, Y. Losovyj, X. Zhang, P. A Dowben, O. F. Mohammed, E. H. Sargent and O. M. Bakr, *Science*, 2015, **347**, 519.
44 A. Buin, P. Pietsch, J. Xu, O. Voznyy, A. H. Ip, R. Comin and E. H. Sargent, *Nano Lett.*, 2014, **14**, 6281.
45 M. L. Agiorgousis, Y.-Y. Sun, H. Zeng and S. Zhang, *J. Am. Chem. Soc.*, 2014, **136**, 14570.
46 W.-J. Yin, T. Shi and Y. Yan, *Appl. Phys. Lett.*, 2014, **104**, 063903.
47 S. De Wolf, J. Holovsky, S.-J. Moon, P. Löper, B. Niesen, M. Ledinsky, F.-J. Haug, J.-H. Yum and C. Ballif, *J. Phys. Chem. Lett.*, 2014, **5**, 1035.
48 E. T. Hoke, D. J. Slotcavage, E. R. Dohner, A. R. Bowring, H. I. Karunadasa and M. D. McGehee, *Chem. Sci.*, 2015, **6**, 613.
49 W.-J. Yin, T. Shi and Y. Yan, *Appl. Phys. Lett.*, 2014, **104**, 063903.
50 H. Y. Hsu, C. Y. Wang, A. Fathi, J. W. Shiu, C. C. Chung, P. S. Shen, T. F. Guo, P. Chen, Y. P. Lee and E. W. Diau, *Angew. Chem., Int. Ed.*, 2014, **53**, 9339.
51 J. Hwang, F. Amy and A. Kahn, *Org. Electron.*, 2006, **7**, 387.
52 T.-W. Lee and Y. Chung, *Adv. Funct. Mater.*, 2008, **18**, 2246.
53 J. Wang and C. K. Ober, *Macromolecules*, 1997, **30**, 7560.
54 M. Fahlman, A. Crispin, X. Crispin, S. K. M. Henze, M. P. de Jong, W. Osikowicz, C. Tengstedt and W. R. Salaneck, *J. Phys.: Condens. Matter*, 2007, **19**, 183202.
55 S. Braun, M. P. de Jong, W. Osikowicz and W. R. Salaneck, *Appl. Phys. Lett.*, 2007, **91**, 202108.
56 T.-W. Lee, O. Kwon, M.-G. Kim, S. H. Park, J. Chung, S. Y. Kim, Y. Chung, J.-Y. Park, E. Han, D. H. Huh, J.-J. Park and L. Pu, *Appl. Phys. Lett.*, 2005, **87**, 231106.
57 http://www.heraeus-clevios.com.
58 C. H. Peters, I. T. Sachs-Quintana, J. P. Kastrop, S. Beaupre, M. Leclerc and M. D. McGehee, *Adv. Energy Mater.*, 2011, **1**, 491.